Chemical Engineering Journal 477 (2023) 147179

Contents lists available at ScienceDirect

Chemical Engineering Journal

journal homepage: www.elsevier.com/locate/cej

In-situ construction of Li-Ag/LiF composite layer for long cycled all-solid-state Li metal battery

Qianxiao Fan, Wendi Zhang, Yilong Jin, Dongmei Zhang, Xianglong Meng, Wanxiong Peng, Jinhui Wang, Jinshan Mo, Kai Liu, Lehao Liu, Meicheng Li *

State Key Laboratory of Alternate Electrical Power System with Renewable Energy, School of New Energy, North China Electric Power University, Beijing 10026, China

ARTICLE INFO

Keywords:
Sulfide solid electrolyte
Composite protection layer
Lithium fluoride
Li-Ag alloy

ABSTRACT

All-solid-state lithium batteries employing sulfide solid electrolyte are promising candidates for next generation lithium batteries. Nevertheless, the unstable interface of sulfide solid electrolyte and Li metal has limited the lifespan of sulfide solid state lithium metal batteries. Herein, a composite protection layer composed of Li-Ag/LiF (LAF) is formed on Li metal surface by the in-situ reaction of silver-fluoride (AgF) and Li metal to solve the instability issue of the Li_6PS_5Cl/Lithium interface. The Li-Ag particles act as nucleation sites for Li deposition and LiF can avoid the growth of lithium dendrites. The density function theory (DFT) calculation results show the lithiophilic of Li-Ag alloys and high interfacial energy of LiF/Li_6PS_5Cl interface, proving the superiority of the LAF protection layer. The critical current density of the Li-LAF/ Li_6PS_5Cl/ LAF-Li symmetric battery is 1.6 mA cm^{-2} and the battery achieved a long lifespan of over 3000 h at 0.1 mA cm^{-2} and 0.1mAh cm^{-2} at room temperature. In addition, a high discharge capacity of 139.1mAh/g is obtained in the LiNbO3@LiCoO2/ Li6PS5Cl/ LAF-Li full cell. This work provides a feasible strategy for the interface modification of sulfide all-solid-state Li metal batteries.

1. Introduction

As lithium-ion battery technology keeps on improving, there is a growing requirement for significant energy density. Due to their potential to simultaneously make a breakthrough in realizing considerable energy density and excellent safety, all-solid-state lithium batteries (ASSLBs) have emerged as the focus of intense battery research [1,2]. The most appropriate anode for ASSLBs is thought to be lithium metal for its incomparable advantages in electrochemical potential, density and theoretical capacity [3]. Before using lithium metal as anode, the option of solid-state electrolyte needs to be considered firstly. For the selection of inorganic solid electrolytes, the main choices are perovskite-type electrolyte, halide-type electrolyte and sulfide-type [4]. Among them, sulfide solid electrolytes stand out for their unique advantages in high ionic conductivity, which is favorable for achieving breakthrough in energy density and pretty safe performance of ASSLBs [5]. Particularly, the argyrodites sulfide solid electrolyte (Li_6PS_5Cl) has drawn more and more attention as its low cost of precursors and simple synthesis method [6]. However, the commercialization of sulfide ASSLBs is hindered by the incompatibility of Li_6PS_5Cl (LPSCl) and Li metal [7]. The LPSCl electrolyte will break down for the reaction with Lithium during the cell operations, leading to a gradual increase in interface impedance [8]. At elevated current densities, the side reactions induce the formation of microcracks within the electrolyte, which subsequently propagate and provide pathways for the accumulation of lithium dendrites and finally result in short circuits [9–11].

Lithium dendrite formation is significantly accelerated by the unstable contact of the interface [12]. In previous researches, a variety of attempts have been made to solve these problems. The insertion of an artificial protection layer (organic polymer [13], LiH_2PO_4, LiF [14,15], etc.) seems to be a pretty choice to avoid direct contact and reduce adverse reactions between the lithium anode and solid electrolyte. An alloying anode protection layer can lead a uniform deposition of lithium metal. Hong et al. [16] enhanced the cycling stability of sulfide ASSLBs by importing a Li-Ag intermetallic layer. Wang et al. [17] used a Li_3N-LiF composite layer to prevent the reactions of Li_3PS_4 and lithium metal. Nevertheless, an ideal artificial protection layer needs to meet the requirements of isolating electron transport and guiding the uniform nucleation of lithium [18]. Therefore, developing an effortless and inexpensive process to construct a uniformly distributed multifunctional

* Corresponding author.
E-mail address: mcli@ncepu.edu.cn (M. Li).

https://doi.org/10.1016/j.cej.2023.147179
Received 13 July 2023; Received in revised form 24 September 2023; Accepted 5 November 2023
Available online 9 November 2023

protective layer for Li_6PS_5Cl/Li interface to prevent side reactions and dendritic lithium growth is extremely needed [19].

In this study, we design a protection layer consisted of Li-Ag/LiF to prevent the creation of lithium dendrites through a simple process. By directly applying a solution of silver fluoride (AgF) onto the lithium surface, the Li-Ag/LiF (LAF) protection layer can be obtained. It was proved by DFT calculations that the Li-Ag alloy can guide uniform deposition of lithium. While for LiF, another product of the reaction, is favorable for isolating lithium dendrites in electrolytes. Compared to the symmetric Li/Li_6PS_5Cl/Li cell, the symmetric Li-LAF/Li_6PS_5Cl/LAF-Li cell demonstrates a significant improvement in critical current density (from 0.6 mA/cm^2 to1.6 mA/cm^2) and a prolonged cycling lifespan (from 200 h to over 3000 h at 0.1 mA/cm^2 and 0.1 mAh/cm^2) at room temperature. Furthermore, a high discharge capacity of 139.1mAh/g is obtained in the full battery with LAF anode and $LiNbO_3$@$LiCoO_2$ cathode. The LAF-protection layer functions well at reducing the production of lithium dendrites either in liquid lithium batteries or solid lithium batteries.

2. Results and discussion

2.1. The LAF-protection layer in solid electrolyte system

The schematic diagrams of Li/Li_6PS_5Cl interface and Li-LAF/ Li_6PS_5Cl interface are illustrated in Fig. 1. In Fig. 1a-b, it is depicted that the Li_6PS_5Cl sulfide solid electrolyte undergoes decomposition when Li metal is utilized as anode, resulting in the creation of a series of byproducts consisting of Li_2S, Li_3P, and LiCl. Dendritic lithium will gradually accumulate as a consequence of adverse effects, which will increase the interface resistance [20]. Therefore, we put forward a Li-Ag/LiF (LAF) protection layer on Li anode through a facile route. As depicted in Fig. 1c-d, the presence of Ag nanoparticles facilitates the uniform deposition of lithium, while LiF acts as a barrier to prevent electron tunneling, thereby ensuring a homogeneous distribution of the electric field [21,22]. Therefore, the compatibility of LPSCl and Li metal is significantly enhanced, which was demonstrated by the results of electrochemical tests.

The LAF-protection layer was established through a facile way. Li-Ag/LiF is established on the surface of lithium metal by exposing Li to AgF solution (DMSO as solvent) and heating at 100 ℃ for an hour to remove the solvent. Firstly, DMSO is stable with lithium metal. Silver fluoride is well dissolved in DMSO. For these two reasons, DMSO is chosen as the solvent. During the heating process, lithium metal will undergo a strong substitution reaction with silver fluoride, forming a protection layer on the outside layer of lithium metal. The DMSO is also removed during the heating process. The main reaction is as followed: Li + AgF → Ag + LiF. The reaction among Li metal and AgF solution is clearly evident when the solution is dropped to the outside layer of Li metal, causing the transformation of the metal surface from silver-like to brown (Fig. S1). The optical microscope image of the Li metal without the LAF protection layer was shown in Fig. 2a. To further prove the construction of Li-Ag/LiF protection layer on the outside of lithium metal, optical microscope, scanning electron microscopy (SEM) and energy dispersive X-ray photoelectron spectroscopy (XPS) were used for analysis. The optical microscope results reveled that the lithium metal turned from silver to orange-yellow (Fig. S2). The surface topography of untreated lithium and the LAF protective layer were observed under SEM, and the surface morphology of LAF layer was uniform (Fig. 2b). FIB-SEM analysis was utilized to assess the thickness of the LAF protection layer, which was found to be 2.8 μm (Fig. 2c), which is the best thickness of the LAF protection layer. The measurements of the best thickness for the protection layer was shown in Fig. S3-S6. We obtained different thickness protective layers by changing the concentration of silver fluoride solution. The concentrations are 0.1 mg/ml,0.3 mg/ml and 0.6 mg/ml, corresponding to the thickness of 1.47 μm, 2.8 μm and 3.855 μm (Fig. S3– 5). To get the best thickness of the protection layer, Lithium symmetric batteries were assembled to measure CCD. As shown in Fig. S7, the CCD varied form 1.3 mA cm^{-2}, 1.6 mA^{-2} to 1.2 mA cm^{-2}. Therefore, the best thickness of the LAF protection layer is 2.8 μm. The ionic conductivity of the Li_6PS_5Cl sheet is 3.4 mS cm^{-1} (Fig. S6).

During the test of EDS elemental mapping, the mapping images of Ag and F (Fig. 2d-e) showed uniform distribution on the protection layer. In addition, the XPS results confirmed the Li-Ag alloy and LiF protection layer was successfully coated on Li. For the sake of further determine the

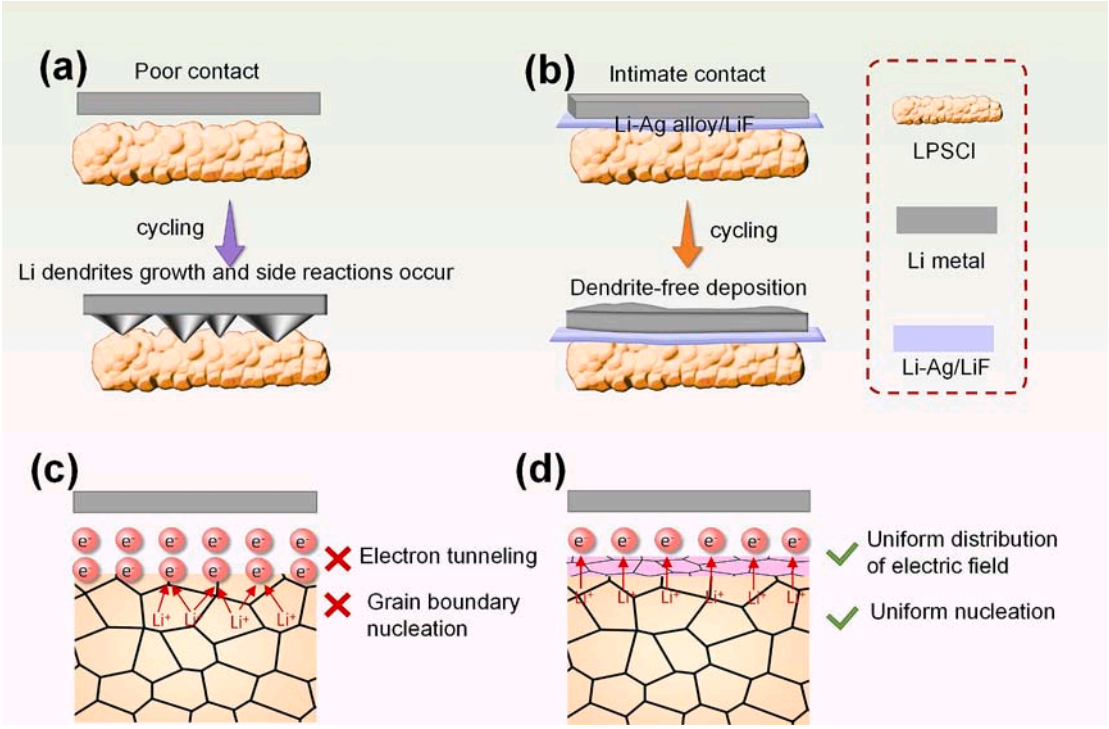

Fig. 1. Schematic illustration of the cycling process (a-b). and Li-ion deposition process (c-d). of Li/Li_6PS_5Cl interface and Li-LAF/ Li_6PS_5Cl interface.

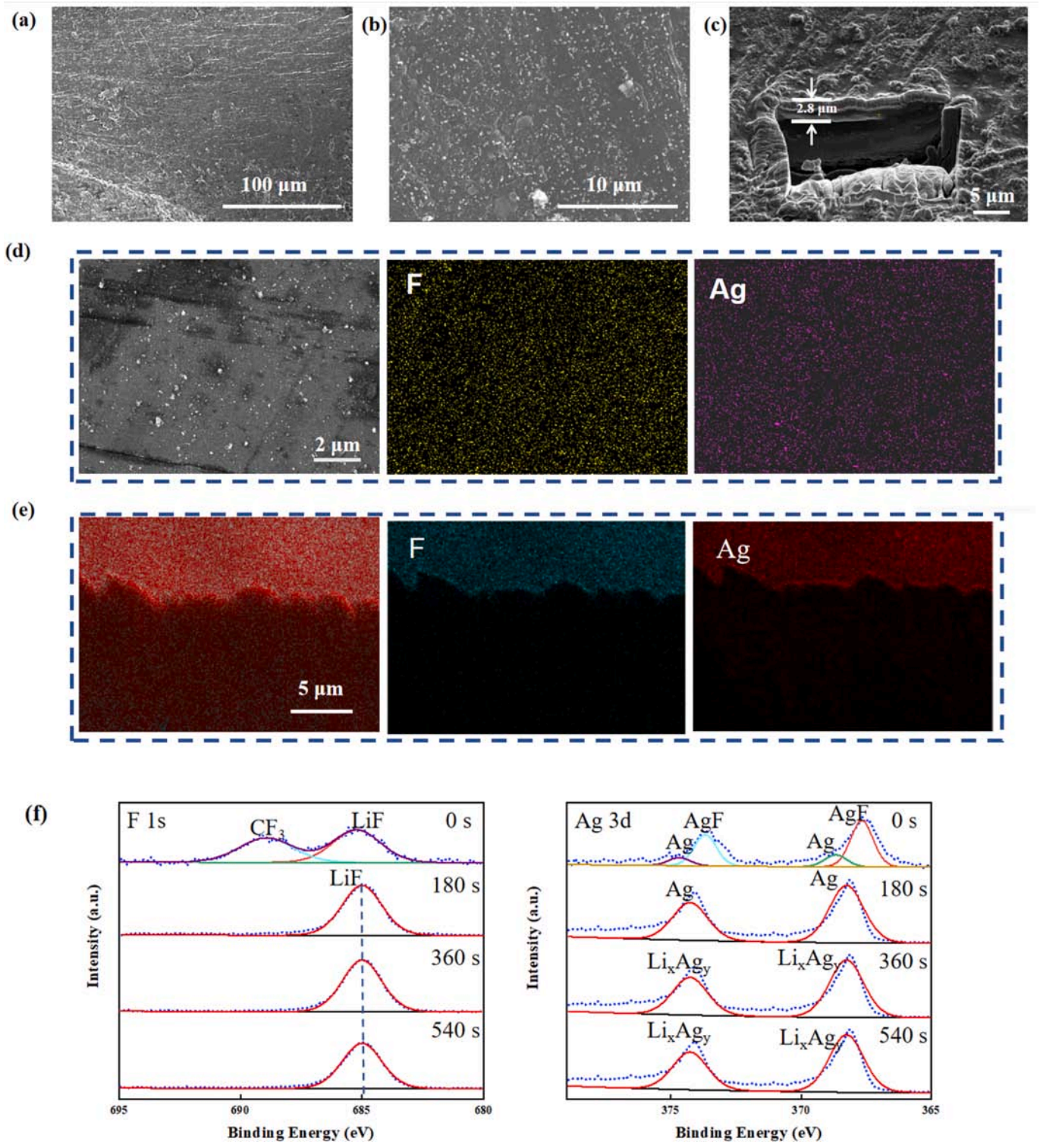

Fig. 2. Characteristic of Lithium metal with and without LAF protection layer. (a-b) SEM image on the top surface of lithium metal without (a) and with (b) the LAF protection layer; (c) FIB-SEM image of the cross section of LAF protection layer; (d) the top surface elemental mappings of the LAF layer; (e) the cross section elemental mappings of the LAF layer; (f) Ag 3d, F 1 s XPS depth spectra XPS results on the surface of AgF treated lithium metal.

element distribution of the LAF layer, XPS profiles were collected from different depth. As shown in Fig. 2f, the Ag 3d XPS spectrum turns out to be excellent spin–orbit components with two peaks at 367.6 and 373.6 eV, matching well with the binding energies of AgF $3d_{3/2}$ and AgF $3d_{5/2}$ when the detaching time is 0 s, respectively [23,24]. The other two peaks at 372.8 and 378.2 eV matches well with Ag $3d_{3/2}$ and Ag $3d_{5/2}$ [25]. When the sputtering time was increased to 180 s, the peaks shift to 368.2 and 374.2 eV, indicating the presence of Ag metal. When the sputtering time is further increased to 360 s and 540 s, the Ag 3d spectrum turns out to be 368.1 and 364.1 eV, corresponding to the intensity of Li_xAg_y. For the element F, two peaks in the F 1 s (Fig. 2f) spectra, matching well with the Li-F in LiF and C-F in -CF_3, were observed at binding energy of 686.5 eV and 688.3 eV [26]. When increasing the sputtering time to 180 s, 360 s and 540 s, there turns out

to be one peak at the binding energy of 686.5 eV, corresponding Li-F in LiF. The XPS depth profiles prove the gradient distribution of element Ag and F in the LAF-Li surface. Through the SEM and XPS characterizations, it is proved that the main ingredients of AgF reacting with Li metal are Li-Ag alloy and LiF.

To validate the protective efficacy of this composite interfacial layer, several electrochemical tests were carried out. Lithium symmetric batteries were used to examine LAF layer affected the critical current density (CCD) [27,28]. As shown in Fig. 3a-b, the CCD value was 0.6 mA cm^{-2} at 25℃ for the cell assembled with untreated lithium tablets and 1.6 mA cm^{-2} at 25℃ for the cell assembled with LAF-coated lithium tablets, proving that the LAF layer is beneficial in solving the unstable interface issue of ASSLBs. To further investigate the role of this protective layer, a long-term cycle test with constant current charge and discharge was performed using the lithium symmetric cell. A symmetric cell was made using the untreated lithium tablets and LPSCl electrolyte for a constant current charge/discharge test (0.1 mA cm^{-2}, 0.1 mAh cm^{-2}). A short circuit caused the failing of the cell after 200 h of cycling (Fig. 3d). This indicated that the dendrites had penetrated the inside of the electrolyte, leading to the voltage drop. In contrast, when tested under the same conditions using a symmetric cell assembled from lithium tablets with LAF protective layer, the cell demonstrated stable cycling more than 3000 h while holding a low overpotential. (Fig. 3c). At the current density of 0.5 mA cm^{-2}, 0.5 mAh cm^{-2}, the Li-LAF/ Li_6PS_5Cl /LAF-Li battery can achieve the stable cycling of over 400 h (Fig. S8). The impedance of the lithium symmetric cell was also measured (Fig. S9). The impedance of the Li-LAF/ Li_6PS_5Cl /LAF-Li battery is much smaller than the impedance of Li/ Li_6PS_5Cl /Li battery. The partial enlargement of Li-LAF/ Li_6PS_5Cl /LAF-Li battery (Fig. 3e) proves that the cell is stable even after the cycling of two thousand hours.

To further confirm the effectiveness of the LAF protection layer, density functional theory (DFT) calculations were employed to determine the interface energy of Li/Li_6PS_5Cl, LiAg/Li_6PS_5Cl and LiF/ Li_6PS_5Cl. As illustrated in the Fig. 4a-c, the interface formation energy of Li/Li_6P_5Cl、LiAg/Li_6PS_5Cl and LiF/Li_6PS_5Cl is 1.2172, 0.4301 and

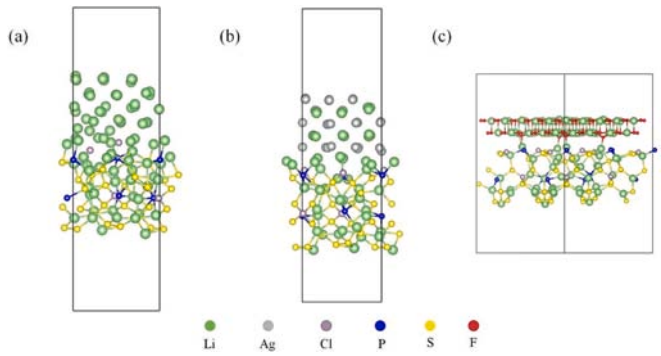

Fig. 4. Schematic illustration of the structure of the DFT calculation. (a) Li (001)/Li_6PS_5Cl (001); (b) LiAg(001)/Li_6PS_5Cl (001);(c) LiF(100)/ Li_6PS_5Cl(001).

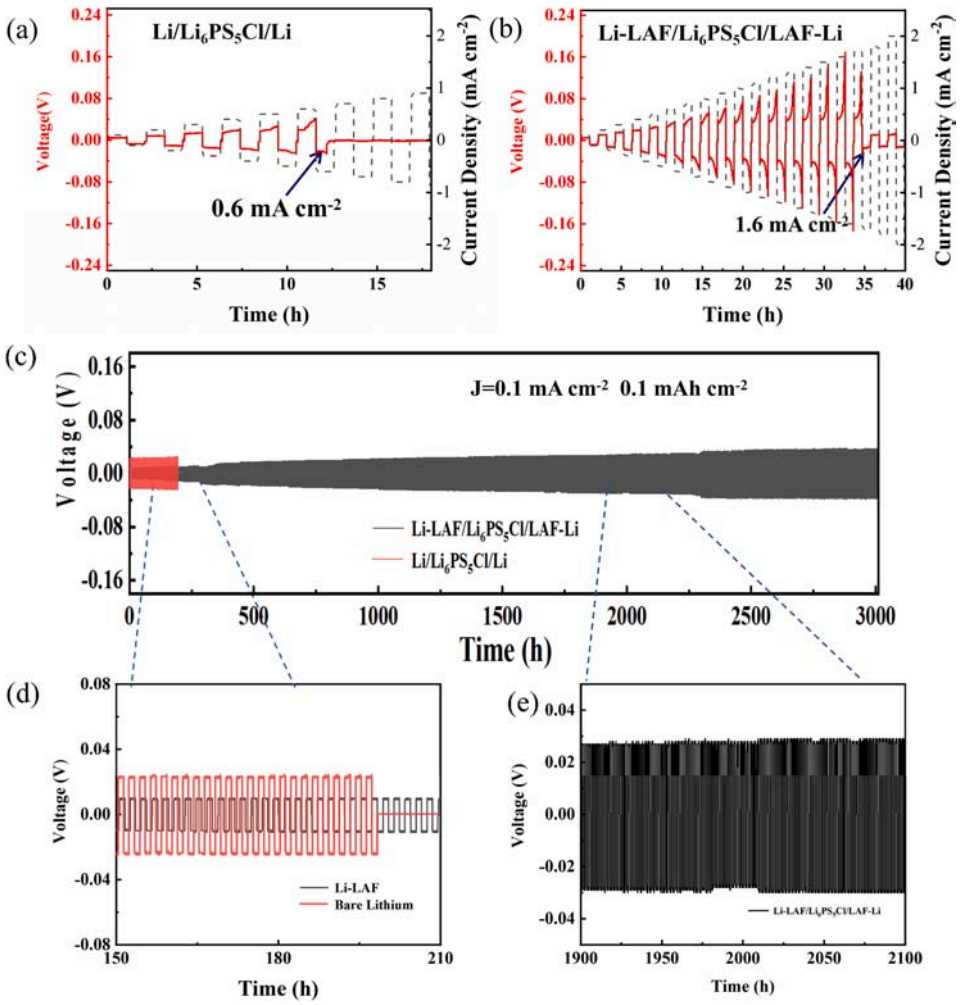

Fig. 3. Lithium symmetric cells tests. (a-b) CCD test; (c) Constant current charge/discharge test; (d-e) partial magnification.

3.0077 J cm^{-2}, correspondingly. Due to the low interfacial energy of the LiAg (001)-Li_6PS_5Cl (001) interface, the Li-Ag alloy layer forms spontaneously on the outside surface of Li metal, and the Ag particles can act as efficient locations of nucleation for the deposition of Li, thus promoting the reduction of Li^+ and achieving the homogeneous deposition of Li metal. The LiF (001)/Li_6PS_5Cl (001) interface has a high interfacial energy, thus the LiF is generated between the Li-Ag alloy layer and the Li_6PS_5Cl electrolyte. As an electronic insulating material, LiF can effectively avoid electron tunneling effect. The elevated interfacial energy substantially raises energy barrier associated with even nucleation, and the high interfacial tension also inhibits the propagation and penetration of Li into the pores and cracks in sulfide electrolyte, thus helping to prevent the accumulation of Li dendrites [29]. All in all, the DFT calculation results further verifies that the LAF protection layer can significantly strengthen the interface stability of Li_6PS_5Cl/Li.

To demonstrate the application of the LAF protection layer in ASSLBs, the LAF-Li anode was combined with $LiNbO_3$-coated $LiCoO_2$ (LNO@LCO) to assemble ASSLBs. The cycling performance of ASSLBs with positive active materials loading of 13.1 mg cm^{-2} using Li_6P_5Cl SSEs (labeled as Li-LAF/ Li_6P_5Cl /LNO@LCO and Li/ Li_6P_5Cl / LNO@LCO, respectively) were tested from 2.5 V to 4.3 V at 0.1C rate. As shown in Fig. 5, the half-cells with the protective layer had a higher first-cycle discharge capacity and a significantly higher average coulombic efficiency than the control group. During the subsequent long cycle test, comparing the experimental and control groups, the former was noticeably more stable (Fig. 5b). A significant increase in capacity retention of about 30 % is achieved in the modified sample (Fig. 5c-d). The Coulombic Efficiencies along with the cycles are provided in Fig. S10. Nevertheless, the electrode material expands in bulk during cell cycling which will create cracks and pores and result in a large interfacial impedance between the solid–solid interface. There is still room for improvement in the cycling stability in whole cell testing. Further improvements will be made to address these issues in subsequent experiments. The comparisons of the recent results in the relative references on the improvement of the electrolyte/Li interface using the strategy of construction the artificial SEI are listed on Table S1.

To explore the detail reasons of the poor cycle performance of the $LiCoO_2$-based full cell without LAF protection layer. We observed the morphologies of the cycle anodes from the $LiCoO_2$-based full cells. Fig. S11 is the lithium anode image disassembled from the cycled Li/ Li_6PS_5Cl/LNO@LCO cell. The formation of lithium dendrites can be observed during the cycling process. In addition, the LPSCl powder sticking to the surface of Li metal is also clearly visible [7]. During the cycling process there are a serious of side reactions between LPSCl and Li metal, which leads to the decomposition and pulverization of LPSCl. While for the Li-LAF anode disassembled from Li-LAF/ Li_6PS_5Cl/ LNO@LCO cell after the cycling of 30 cycles, the surface of Li-LAF is relative smooth (Fig. S12). Both lithium dendrites and LPSCl powder are not observed. The surface topography of LPSCl sheet after cycling was also observed. As shown in Fig. S13. These results further confirm the effectiveness of LAF protection layer in improving the interface stability of lithium and Li_6PS_5Cl.

2.2. The LAF protection layer in liquid electrolyte system

In liquid electrolyte systems, the longevity of the lithium metal

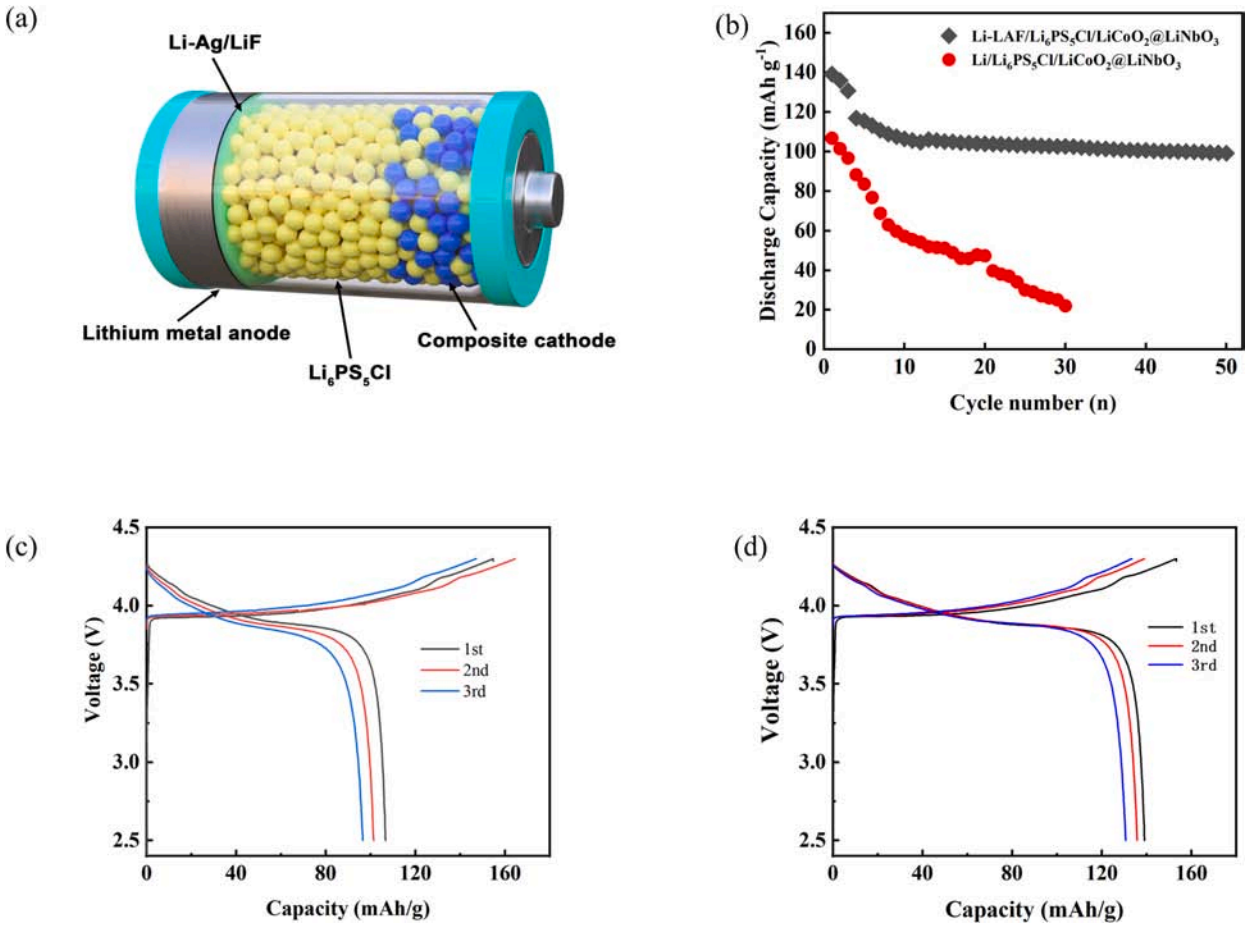

Fig. 5. Schematic illustration of the full cell. (a) Schematic diagram of all-solid-state battery; (b) Cycling performance of LNO@LCO/Li_6PS_5Cl/Li and LNO@LCO/ Li_6PS_5Cl /LAF-Li at 0.1C; (c) Charge/discharge potential curves of LNO@LCO/ Li_6PS_5Cl /Li at 0.1C; (d) Charge/discharge potential curves of LNO@LCO/ Li_6PS_5Cl /LAF-Li at 0.1C.

battery is constrained by uncontrolled reactions occurring between lithium metal and non-aqueous electrolytes. Li-Li symmetric cells were tested in liquid electrolyte systems to determine the efficacy of the LAF-protection layer.

The cycling process of bare lithium anode and Li-LAF anode in liquid electrolyte systems is shown in Fig. S14. For the lithium metal batteries without artificial layer, uncontrolled side reactions will occur and result in the accumulation of lithium dendrites (Fig. S14b). Conversely, the inclusion of Ag nanoparticles in the LAF layer promotes the homogeneous deposition of Li ions on the outside of lithium metal, while LiF impedes the growth of lithium dendrites. As a result of these factors, a dendrite free morphology is observed after the deposition of Li ions for several hours (Fig. S14c).

To further validate the effect of the LAF protection layer, a variety of electrochemical tests were carried out in the symmetric Li/Li cells at varied current densities. Fig. S15a showed the voltage profiles over time (0.25 mA cm^{-2} and 0.25 mAh cm^{-2}). It is evident that the polarization voltage of lithium metal symmetric battery after silver fluoride treatment decreases gradually and approaches a stable value, and there is a small overpotential in the stable stage (Fig. S15). At larger current densities (1.5 mA cm^{-2} and 1.5 mAh cm^{-2}), the cycling stability of symmetric cells was investigated. The LAF-Li/Li-LAF cells are stable even after the Li plating/striping cycles of 1000 h. Conversely, the cells without the LAF protection layer failed within 400 h (Fig. S15b). The cell with LAF protection layer behaved lower polarization at various current densities (Fig. S15).

Electrochemical impedance spectroscopy (EIS) tests were made to establish the significant impact of the LAF protective layer on stabilizing the lithium metal anode. The measurements were performed from 5 cycles to 50 cycles at a current density of 1 mA cm^{-2} and a capacity of 1 mAh cm^{-2}. The impedance of the Li/Li symmetrical cell (Fig. S16b) exhibited initial higher values during the first few cycles, which gradually decreased during the cycling. Conversely, the impedance of Li-LAF/LAF-Li symmetrical cell (Fig. S16a) was particularly small during the whole cycling process, proving that the LAF protection layer is favorable for the formation of an ideal artificial layer. The above analysis confirms that treating the lithium anode with silver fluoride is a viable approach to construct a stable interface for a dendrite-free Li metal battery.

To investigate the morphological evolution of LAF electrode, the SEM images of LAF electrode were observed, which is favorable for understanding the reason behind the improvement of interface stability. The images of Li plating/stripping were observed. After 100 cycles at 2.5 mA cm^{-2} for the untreated Li anode, cellular dendrites were observed on the Li-planted side and cracks occurred on the Li-stripped side (Fig. S17a-c). In contrast, the aspect of the silver fluoride treated lithium was smooth and flat after 200 h cycling, and no root whisker-like dendrites appeared (Fig. S17d-f). The EDS mapping of the cycled Li-LAF was made to identify whether the protection layer is destroyed. The presence of element F and Ag proved that the protection layer was not broken after cycling (Fig. S17h-i). The white shinning points in Fig. S17g represented element Ag. These results further verified the role of LAF-protection layer in long cycled lithium metal batteries. According to the results mentioned above, LAF-protection layer is also effective for the suppression of lithium dendrites in liquid electrolyte systems.

3. Conclusion

In summary, a composite protection layer made of Li-Ag/LiF (LAF) was formed on the surface of lithium by reacting AgF and Li metal, effectively solving the instability issue of Li/Li_6PS_5Cl interface. The formation process of Li-Ag/LiF through the replacement of AgF with Li metal is confirmed through SEM and XPS characterizations. The presence of Li-Ag alloys significantly enhances the interface stability of the Li/Li_6PS_5Cl interface and make it easier to deposit Li ions evenly. Additionally, the inclusion of LiF effectively inhibits the nucleation and growth of lithium dendrites at the interface. The combination of LiF and Li-Ag alloys enhanced the compatibility of Li/Li_6PS_5Cl interface, resulting in a decrease in interface resistance. Therefore, the Li-LAF/Li_6PS_5Cl/LAF-Li symmetric cell can stably cycle over 3000 h with a low overpotential (36 mV). When combined with LNO@LCO cathode, the Li-LAF/ Li_6PS_5Cl/LNO@LCO cell demonstrated a high initial capacity of 139.11 mAh/g with superior cycling stability at 30 ℃. These exceptional electrochemical performances highlight the effectiveness of the designed Li-Ag/LiF protection layer in suppressing lithium propagation into the sulfide solid-state electrolytes. A stable lithium metal anode was also prepared in liquid electrolyte systems with excellent cycling stability (over 1000 h at 1.5 mA cm^{-2} and 1.5 mAh cm^{-2}) for the Li-LAF|| LAF-Li symmetric battery. This study presents a straightforward approach to enhance the interface compatibility between lithium metal and Li_6PS_5Cl sulfide solid electrolyte.

4. Experiment section

4.1. Sample synthesis

The Li_6PS_5Cl powder were purchased from Shenzhen Kejing Company.

The AgF solution was obtained by dissolving 3 mg AgF (Alfa Aesar, 99.8 %) in DMSO solution (Sigma Aladdin,99.8 %). To obtain the LAF protection layer, the surface of the lithium foil is evenly coated with 40 Âμl solution dropped by pipette gun. Then the coated lithium foil was heated at 100 ℃ for 1 h to remove the solution, during which Li will react with AgF and generates Ag and LiF. All the samples were prepared within a glovebox filled with argon gas.

4.2. Material characterization

The sample morphologies were analyzed utilizing a Hitachi SU-70 field-emission SEM. Additionally, the FIB-SEM morphologies were acquired using the Thermo Scientific Scios 2 DualBeam system. XPS analysis was performed using a Kratos Axis 165 spectrometer equipped with a monochromatic Al Kα X-ray radiation source.

4.3. Cell measurement

120 mg of Li_6PS_5Cl powder was cold-pressed at 360 MPa to create a sheet. The powder was placed in a PTFE tank, the diameter of which was 10 mm. The thickness of the LPSCl sheet was approximately 1 mm. In order to achieve intimate contact among Li foil and Li_6PS_5Cl electrolyte, Li foils with a 10 mm diameter were affixed to both faces of the electrolyte sheet. For the cells in liquid electrolyte systems, the Li-Ag/LiF anodes were placed at both sides of the separator. The Cellgard 2000 separator was used as the separator. The electrolyte was formulated by combining ethylene carbonate (EC) and dimethyl carbonate (DMC) in a 1:1 vol ratio, with a concentration of 1.0 M $LiPF_6$. The detailed assemble process of all-solid-state lithium cells is shown in the Supplementary materials. The electrochemical tests are shown in Supplementary materials.

4.4. Calculation

Detailed calculations are provided in the Supplementary materials.

Declaration of Competing Interest

The authors declare that they have no known competing financial interests or personal relationships that could have appeared to influence the work reported in this paper.

Data availability

Data will be made available on request.

Acknowledgements

This work is supported partially by project of State Key Laboratory of Alternate Electrical Power System with Renewable Energy Sources (LAPS21004, LAPS202114), National Natural Science Foundation of China (Grant nos. 52272200, 51972110, 52102245 and 52072121), Beijing Science and Technology Project (Z211100004621010), Beijing Natural Science Foundation (2222076, 2222077), Hebei Natural Science Foundation (E2022502022), Huaneng Group Headquarters Science and Technology Project (HNKJ20-H88), 2022 Strategic Research Key Project of Science and Technology Commission of the Ministry of Education, China Postdoctoral Science Foundation (2022M721129) and the Fundamental Research Funds for the Central Universities (2022MS030, 2021MS028, 2020MS023, 2020MS028) and the NCEPU "Double First-Class" Program.

Appendix A. Supplementary data

Supplementary data to this article can be found online at https://doi.org/10.1016/j.cej.2023.147179.

References

[1] C. Wu, J. Lou, J. Zhang, Z. Chen, A. Kakar, B. Emley, Q. Ai, H. Guo, Y. Liang, J. Lou, Y. Yao, Z. Fan, Current status and future directions of all-solid-state batteries with lithium metal anodes, sulfide electrolytes, and layered transition metal oxide cathodes, Nano Energy 87 (2021), 106081.
[2] L. Ye, X. Li, A dynamic stability design strategy for lithium metal solid state batteries, Nature 593 (2021) 218–222.
[3] W. Zhang, Q. Fan, D. Zhang, L. Liu, S. Liu, Z. Fang, W. Li, X. Li, M. Li, Dynamic charge modulate lithium uniform plating functional composite anode for dendrite-free lithium metal batteries, Nano Energy 102 (2022), 107677.
[4] J. Wu, S. Liu, F. Han, X. Yao, C. Wang, Lithium/Sulfide All-Solid-State Batteries using Sulfide Electrolytes, Adv. Mater. 33 (2021) e2000751.
[5] C. Wang, J. Liang, Y. Zhao, M. Zheng, X. Li, X. Sun, All-solid-state lithium batteries enabled by sulfide electrolytes: from fundamental research to practical engineering design, Energ. Environ. Sci. 14 (2021) 2577–2619.
[6] J.E. Lee, K.-H. Park, J.C. Kim, T.-U. Wi, A.R. Ha, Y.B. Song, D.Y. Oh, J. Woo, S. H. Kweon, S.J. Yeom, W. Cho, K. Kim, H.-W. Lee, S.K. Kwak, Y.S. Jung, Universal Solution Synthesis of Sulfide Solid Electrolytes Using Alkahest for All-Solid-State Batteries, Adv. Mater. 34 (2022) 2200083.
[7] D. Zeng, J. Yao, L. Zhang, R. Xu, S. Wang, X. Yan, C. Yu, L. Wang, Promoting favorable interfacial properties in lithium-based batteries using chlorine-rich sulfide inorganic solid-state electrolytes, Nat. Commun. 13 (2022) 1909.
[8] Y. Zhu, X. He, Y. Mo, First principles study on electrochemical and chemical stability of solid electrolyte–electrode interfaces in all-solid-state Li-ion batteries, J. Mater. Chem. A 4 (2016) 3253–3266.
[9] Y. Lu, C.-Z. Zhao, H. Yuan, X.-B. Cheng, J.-Q. Huang, Q. Zhang, Critical Current Density in Solid-State Lithium Metal Batteries: Mechanism, Influences, and Strategies, Adv. Funct. Mater. 31 (2021) 2009925.
[10] Z. Liang, Y. Xiang, K. Wang, J. Zhu, Y. Jin, H. Wang, B. Zheng, Z. Chen, M. Tao, X. Liu, Y. Wu, R. Fu, C. Wang, M. Winter, Y. Yang, Understanding the failure process of sulfide-based all-solid-state lithium batteries via operando nuclear magnetic resonance spectroscopy, Nat. Commun. 14 (2023) 259.
[11] S. Luo, X. Liu, X. Zhang, X. Wang, Z. Wang, Y. Zhang, H. Wang, W. Ma, L. Zhu, X. Zhang, Nanostructure of the Interphase Layer between a Single Li Dendrite and Sulfide Electrolyte in All-Solid-State Li Batteries, ACS Energy Lett. 7 (2022) 3064–3071.
[12] R. Song, J. Yao, R. Xu, Z. Li, X. Yan, C. Yu, Z. Huang, L. Zhang, Metastable Decomposition Realizing Dendrite-Free Solid-State Li Metal Batteries, Adv. Energy Mater. 13 (2023) 2203631.
[13] W. Zhou, S. Wang, Y. Li, S. Xin, A. Manthiram, J.B. Goodenough, Plating a Dendrite-Free Lithium Anode with a Polymer/Ceramic/Polymer Sandwich Electrolyte, J. Am. Chem. Soc. 138 (2016) 9385–9388.
[14] H. Su, Y. Liu, Y. Zhong, J. Li, X. Wang, X. Xia, C. Gu, J. Tu, Stabilizing the interphase between Li and Argyrodite electrolyte through synergistic phosphating process for all-solid-state lithium batteries, Nano Energy 96 (2022), 107104.
[15] R. Xu, F. Han, X. Ji, X. Fan, J. Tu, C. Wang, Interface engineering of sulfide electrolytes for all-solid-state lithium batteries, Nano Energy 53 (2018) 958–966.
[16] H.J. Choi, D.W. Kang, J.W. Park, J.H. Park, Y.J. Lee, Y.C. Ha, S.M. Lee, S.Y. Yoon, B.G. Kim, In Situ Formed Ag-Li Intermetallic Layer for Stable Cycling of All-Solid-State Lithium Batteries, Adv. Sci. (Weinh.) 9 (2022) e2103826.
[17] X. Ji, S. Hou, P. Wang, X. He, N. Piao, J. Chen, X. Fan, C. Wang, Solid-State Electrolyte Design for Lithium Dendrite Suppression, Adv. Mater. 32 (2020) e2002741.
[18] C. Wang, T. Deng, X. Fan, M. Zheng, R. Yu, Q. Lu, H. Duan, H. Huang, C. Wang, X. Sun, Identifying soft breakdown in all-solid-state lithium battery, Joule 6 (2022) 1770–1781.
[19] H. Wan, J. Zhang, J. Xia, X. Ji, X. He, S. Liu, C. Wang, F and N Rich Solid Electrolyte for Stable All-Solid-State Battery, Adv. Funct. Mater. 32 (2022) 2110876.
[20] A. Banik, Y. Liu, S. Ohno, Y. Rudel, A. Jiménez-Solano, A. Gloskovskii, N. M. Vargas-Barbosa, Y. Mo, W.G. Zeier, Can Substitutions Affect the Oxidative Stability of Lithium Argyrodite Solid Electrolytes? ACS Appl. Energy Mater. 5 (2022) 2045–2053.
[21] S. Jin, Y. Ye, Y. Niu, Y. Xu, H. Jin, J. Wang, Z. Sun, A. Cao, X. Wu, Y. Luo, H. Ji, L. J. Wan, Solid-Solution-Based Metal Alloy Phase for Highly Reversible Lithium Metal Anode, J. Am. Chem. Soc. 142 (2020) 8818–8826.
[22] F. Zhao, Q. Sun, C. Yu, S. Zhang, K. Adair, S. Wang, Y. Liu, Y. Zhao, J. Liang, C. Wang, X. Li, X. Li, W. Xia, R. Li, H. Huang, L. Zhang, S. Zhao, S. Lu, X. Sun, Ultrastable Anode Interface Achieved by Fluorinating Electrolytes for All-Solid-State Li Metal Batteries, ACS Energy Lett. 5 (2020) 1035–1043.
[23] Z. Peng, J. Song, L. Huai, H. Jia, B. Xiao, L. Zou, G. Zhu, A. Martinez, S. Roy, V. Murugesan, H. Lee, X. Ren, Q. Li, B. Liu, X. Li, D. Wang, W. Xu, J.-G. Zhang, Enhanced Stability of Li Metal Anodes by Synergetic Control of Nucleation and the Solid Electrolyte Interphase, Adv. Energy Mater. 9 (2019) 1901764.
[24] Y. Jiang, Q. Lv, C. Bao, B. Wang, P. Ren, H. Zhong, Y. Yang, X. Liu, Y. Dong, F. Jin, D. Wang, T. Xiong, H. Liu, S. Dou, J. Wang, J. Xue, Seamless alloying stabilizes solid-electrolyte interphase for highly reversible lithium metal anode, Cell Rep. Phys. Sci. 3 (2022), 100785.
[25] L.-N. Wu, J. Peng, F.-M. Han, Y.-K. Sun, T. Sheng, Y.-Y. Li, Y. Zhou, L. Huang, J.-T. Li, S.-G. Sun, Suppressing lithium dendrite growth by a synergetic effect of uniform nucleation and inhibition, J. Mater. Chem. A 8 (2020) 4300–4307.
[26] B. Zhong, J. Wu, L. Ren, T. Zhou, Z. Zhang, W. Liu, H. Zhou, Constructing a lithiophilic and mixed conductive interphase layer in electrolyte with dual-anion solvation sheath for stable lithium metal anode, Energy Storage Mater. 50 (2022) 792–801.
[27] J. Kasemchainan, S. Zekoll, D. Spencer Jolly, Z. Ning, G.O. Hartley, J. Marrow, P. G. Bruce, Critical stripping current leads to dendrite formation on plating in lithium anode solid electrolyte cells, Nat. Mater. 18 (2019) 1105–1111.
[28] S. Sarkar, V. Thangadurai, Critical Current Densities for High-Performance All-Solid-State Li-Metal Batteries: Fundamentals, Mechanisms, Interfaces, Materials, and Applications, ACS Energy Lett. 7 (2022) 1492–1527.
[29] Z. Wu, C. Wang, Z. Hui, H. Liu, S. Wang, S. Yu, X. Xing, J. Holoubek, Q. Miao, H. L. Xin, P. Liu, Growing single-crystalline seeds on lithiophobic substrates to enable fast-charging lithium-metal batteries, Nat. Energy 8 (2023) 340–350.